A novel disk-type X-ray area imaging detector using radiophotoluminescence in silver-activated phosphate glass

doi: 10.1016/j.radmeas.2012.09.003

A novel disk-type X-ray area imaging detector using radiophotoluminescence in silver-activated phosphate glass

Toshio Kurobori*, Shoichi Nakamura

Graduate School of Natural Science & Technology, Kanazawa University, Kakuma, Kanazawa 920-1192, Japan

Abstract

We report a novel two- and three-dimensional (2-D, 3-D) imaging detector based on the radiophotoluminescence (RPL) phenomenon in silver-activated phosphate glass (PG:Ag) and evaluate its dosimetric characteristics. A compact disk-type PG:Ag detector with a diameter of 80 mm was rotated at a rate of 400 rpm to read out the accumulated dose information and then remove the images for reuse. After X-ray exposure, three RPL dosimeter processes, i.e., preheating, reading, and erasing, were carried out with only a UV laser at 375 nm by adjusting the stepwise output levels. The 3-D images and dose distributions were rapidly reconstructed with a high spatial resolution of 1 μm and a sensitivity of 1 mGy.

Keywords:
Glass dosimeter, X-ray imaging, Radiophotoluminescence (RPL), Silver defect clusters , Ag-doped phosphate glass

PACS code:

29.40.Wk, 87.59.-e, 61.72.jn, 78.60.-b, 61.80.Ba, 78.47.jd

---

*Corresponding author: Phone: +81 76 264 5478, Fax: +81 76 234 4132.
E-mail address: kurobori@staff.kanazawa-u.ac.jp (T. Kurobori).

1. Introduction

The radiophotoluminescent glass dosimeter (RPLGD) (Perry, 1987; Ranogajec-Komor et al., 2008) using silver-activated phosphate glass (PG:Ag) has been widely used for personal, environmental and clinical dosimetry, as has the optically stimulated luminescence dosimeter (OSLD) (Yukihara and McKeever, 2011) and the thermoluminescent dosimeter (TLD) (Oberhofer and Scharmann, 1979; Olko, 2010). In particular, the RPLGD has been recognized as possessing desirable characteristics such as repeated (nondestructive) readout capabilities, a long-term stability against fading, a wide dynamic range, a low detection threshold, and uniformity/batch homogeneity (Knežević et al., 2011; Lee et al., 2009). Though the RPLGD has the above-mentioned advantages over the OSLD and TLD, these advantages have not led to the use of the RPLGD in two- and three-dimensional (2-D, 3-D) imaging applications and dose distributions.

The photostimulable phosphor screen, $BaFX:Eu^{2+}$ (X=Br, Cl, I), called the imaging plate (Sonoda et al., 1983) has been intensively developed and used successfully in some applications. Moreover, several demonstrations to visualize the stored dose information have been carried out using stable color centers (CCs) in transparent materials. First, the utilization of stable F_2 and F_3^+ CCs in lithium fluoride (LiF) crystals and films as an imaging detector for X-ray microradiographs based on a fluorescence confocal optical microscope has been developed for the extreme ultraviolet (EUV), soft X-ray, and hard X-ray wavelengths produced by various sources (Baldacchini et al., 2003; Bonfigli et al., 2005; Pikuz et al., 2012). Second, the utilization of stable F_2^{2+} (2Mg) CCs in aluminum oxide doped with carbon and magnesium (Al_2O_3:C,Mg) crystals with a 3-D spatial distribution and a fluorescent nuclear track detector (FNTD) based on confocal fluorescent microscopy and a photomultiplier (PMT) has been investigated for various ionizing radiation, high-energy heavy ions, and neutrons (Akselrod et al., 2006a; Akselrod et al., 2006b). Recently, the utilization of radiation-induced silver species, such as Ag^{2+} CCs, in PG:Ag as a 2-D spatial distribution detector (Maki et al., 2011) and a microbeam profiler (Sato et al., 2008) based on confocal fluorescent microscopy and photon counting has been investigated for alpha rays and X-rays, respectively. From a practical point of view, these methods are not suitable for applications outside the laboratory.

The fluorescent CCs of the above-mentioned materials, i.e., LiF, Al_2O_3:C,Mg and PG:Ag, possess superior features, including photothermal stability and desirable physical and chemical properties, even at room temperature. These features also suggest

that higher-temperature thermal annealing processes are necessary to erase such stable CCs. In practice, these detectors require a heat treatment of 400 ºC for 30 min for LiF, 680 ºC for 10 min for Al_2O_3:C,Mg and 400 ºC for 30 min for PG:Ag to render the dosimeter ready for reuse.

In this paper, the CD-type PG:Ag detector system with a high spatial resolution, a high sensitivity on large areas, and a nondestructive readout based on the RPL phenomenon was demonstrated for the first time. In the case of a commercial glass badge, the PG:Ag dosimeter requires a 30 min preheating process at 100 ºC to accelerate the “build-up” and a 30 min annealing process at 400 ºC to erase the stable CCs for reuse. Such heat treatments, which are normally carried out with a furnace, could be accomplished by adjusting the stepwise output power levels up to 70 mW of a cw UV laser at 375 nm. Moreover, the developed system has the same optical pick-up structures of the generally used digital versatile disk (DVD) and Blu-ray Disk (BD).

2. Experimental details

A commercially available PG:Ag dosimeter, GD-450 (AGC Techno Glass), was used as the RPL imaging detector and was cut with an 80 mm diameter and a 1-mm-thick plate. Moreover, the area sizes and forms are not limited due to the functionality and controllability of the host materials. The CD-type PG:Ag plate had a hole with a diameter of 15 mm at the center for rotation. Then, the surface of the PG:Ag was coated with 10-nm-thick Al on one side to increase the temperature effectively. The weight composition of the glass detector was the same as the GD-450 dosimeter and was 31.55% P, 51.16% O, 6.12% Al, 11.00% Na, and 0.17% Ag. All samples were colored by irradiation from an X-ray unit (8.05 keV) with a copper target that was operated at 30 kV and 20 mA. In this work, the samples were irradiated such that the absorbed doses ranged from 1 mGy to 1 Gy.

A collimated UV light at 375 nm from a laser diode was focused on the CD-type X-ray-irradiated PG:Ag rotating at a rate of 400 rpm, and the orange RPL with a peak at 610 nm detected through appropriate optical filters by a photomultiplier tube (H10720, Hamamatsu) was translated from the inside to the outside of the disk in the radial direction. An oscilloscope (Wave Runner 640Zi, LeCroy) was then used to digitize the signal from the PMT, and area fluorescence images were reconstructed by a personal computer (PC).

Optical absorption (OA), excitation (Exc), and emission (Emi) measurements were performed at room temperature using Hitachi U-3900H UV-VIS and F-4500

fluorescence spectrophotometers, respectively. In addition, a time-resolved spectral measurement was carried out with the third harmonic beam at 355 nm from a Q-switched Nd:YAG laser (Surelite I, Hoya-Continuum) and a photonic multichannel analyzer (PMA-12, Hamamatsu).

3. Results and discussion

We previously reported that each X-ray-induced band of PG:Ag was attributed to silver-, phosphorous- and oxygen-related species on the basis of strong analogies with X-ray-irradiated silver-doped sodium chloride (NaCl:Ag) (Kurobori et al., 2010). In addition, the origin, formation kinetics and optical properties were also investigated with a peak-fitting analysis, a high-repetition-rate femtosecond (fs) laser technique, an RPL decay curve analysis, a heat treatment, and transmission electron microscopy (TEM) (Zheng and Kurobori, 2011a; Zheng et al., 2011; Zheng and Kurobori, 2011b).

The OA spectra in PG:Ag with a thickness of 0.3 mm before (curve 1) and after (curve 2) X-ray irradiation under an absorbed dose of 1.0 Gy are shown in Fig. 1(a). After the irradiation, a 30-min preheat was performed at 100 ºC to suppress the 'build-up' kinetics. In addition, the excitation spectra (curves 3 and 4) and the corresponding RPL emission spectra (curves 5-7) are shown. The excitation spectra consisted of two different spectra. One had a peak at 310 nm (curve 3) for an emission spectrum at 560 nm (the orange RPL), and the other peaks at 270 and 345 nm (curve 4) corresponded to a main emission at 470 nm (the blue RPL). As already reported (Kurobori et al., 2010), the former peak at 310 nm was attributed to the Ag^{2+} centers, while the latter peaks at 270 and 345 nm were attributed to Ag_2^{+} and Ag^{0} centers, respectively. Therefore, in this work, the blue emission due to the Ag^{0} centers and some portion of the orange emission due to the Ag^{2+} centers were simultaneously emitted by an excitation wavelength of 375 nm from the laser diode (Zhao et al., 2011). Fig. 1(b) shows the time-resolved spectral measurement made by a multichannel analyzer. The X-ray-irradiated PG:Ag was excited with the third harmonic beam at 355 nm from a Q-switched Nd:YAG laser with a full width at half-maximum intensity (FWHM) of 3 ns and a single pulse energy of 0.3 mJ. The lifetime values at the blue emission at 460 nm and the orange emission at 630 nm were 5.6 ns and 2200 ns, respectively. Note that the red shift of the orange RPL emission was observed from 560 nm by a weak excitation using a fluorescence spectrophotometer to 630 nm by a strong excitation using a UV laser.

A schematic view of the experimental setup for the measurement of the 2-D and 3-D images and dose distributions is shown in Fig. 2. For reading, a cw laser diode with a low-level power of 5 mW at 375 nm was used for stimulating the RPL emission at 630 nm. The laser beam was expanded and reflected with a dichroic beam splitter and was focused on the vicinity of the surface of the PG:Ag plate by a Nikon LU Plan Fluor objective lens (×100, 0.90 NA). The objective lens was simultaneously used both for laser excitation and emission collection. Additional optical filters were inserted to reject residual stimulating laser light and the RPL blue emission at 460 nm. The PG:Ag plate was irradiated by X-rays through the mask and rotated at a maximum speed of 400 rpm. Only the orange RPL was detected by the PMT, and the detector on the X-Y stage was controlled by a PC to translate the beam spot from the inside to the outside of the radial direction. A high-speed oscilloscope was then used to digitize the signal from the PMT, and area fluorescence images were reconstructed by the PC within several minutes.

Fig. 3 shows the relationship between the response of the orange RPL intensity in mV and the X-ray absorbed dose in mGy obtained for rotating the CD-type PG:Ag at a speed of 400 rpm. Twelve different absorbed doses (#1-#12) from 1 mGy to 1 Gy were obtained by using X-ray irradiation covered with a chopping-disk-mask, and the corresponding RPL signal was obtained with the 375 nm laser light. The X-ray irradiated pattern was only visualized under a black light at 352 nm, as shown in the inset. During the measurement, there was no substantial fading of the stored images under a 5 mW power level. The overall results showed a good dose linearity response from 1 mGy to 1 Gy. The value of R^2 was almost unity, 0.998, which shows that the relationship between the orange RPL intensity and absorbed dose is a direct proportion function.

In order to estimate a spatial resolution of the present system, the line pattern with different line-widths (FWHM) was drawn on the surface of the PG:Ag detector by the electron beam using a scanning electron microscope (SEM). The acceleration voltage and the scanning rate were 18 kV and 50 μm/s, respectively. Each line-width drawn by the electron beam was 100, 50, 10, 7, 5, and 1 μm, respectively. In addition, the same line pattern was also taken using the homemade rotating acquisition system at a rotating speed of 400 rpm, as shown in Fig. 4. The RPL bright lines were much wider due to the rotating motion (jitter) of the sample rather than the image blurring (Baldacchini et al., 2003). A schematic view of the spatial resolution measurement is shown in the inset. Only taking into account the single Ag-induced (Ag^0 or Ag^{2+}) color center size, the spatial resolution will be several tens of nanometers. However, in this work, the lateral resolution of the PG:Ag dosimeter with a conventional optical

objective lens was estimated as 0.61λ/NA, where the wavelength λ=630 nm and the numerical aperture NA=0.9, therefore giving a resolution of the order of 400 nm.

Fig. 5 shows a set of images obtained from the proposed RPL glass detector: (a-1) and (a-2) show the photoimages of the mask for X-ray irradiation, (b-1) and (b-2) show the RPL images of the X-ray-irradiated CD-type glass detector illuminated by a black light at 352 nm, and (c-1) and (c-2) show the reconstructed 2-D dose distribution and 3-D image, respectively. It was confirmed from the comparative images that the novel dosimeter system with the RPL PG:Ag has considerable potential for the simultaneous measurement of radiation images and doses. In the present experiments, the diameter of the CD-type PG:Ag detector, rotating speed, increment (pitch), and number of tracks were φ80 mm, 400 rpm (6.7 Hz), 50 μm, and 800 tracks, respectively. Therefore, one image, such as Figs. 5(c-1) and (c-2), was constructed in 2 min with a large dynamic range of 12 bits.

4. Conclusions

The data obtained in this study yielded the following conclusions: a CD-type PG:Ag detector system with a high spatial resolution, a high sensitivity on large areas, and a nondestructive readout was proposed and demonstrated for the first time. In addition, the dosimetric performance and imaging and dose distribution were evaluated with only a single UV laser diode. The developed CD-type glass dosimeter system based on the RPL phenomenon is applicable to the measurement of residual stress in rails by means of the diffraction technique because of its excellent features, such as a compact structure, fast acquisition, and versatile functions. Further improvements to the system, such as using thinner RPL glass plates of less than 0.3 mm in thickness, poly carbonate (PC) base layers, a higher rotating speed up to 2400 rpm (40 Hz), and a cheaper stimulating laser diode at 405 nm instead of a 375 nm laser diode, are being performed.

Acknowledgements

I would like to thank Ms. Y. Miyamoto, Dr. D. Maki, and Dr. T. Yamamoto at Chiyoda Technol Corporation for their contributions to the GD-450 sample preparation and Prof. H. Nanto at Kanazawa Institute of Technology for his fruitful discussions. I would also like to thank Dr. S. Nakamura at Kanazawa University and Mr. N. Zushi at

Osaka University for their contributions to making the reconstructed images and drawing the electron beam pattern, respectively.

FIGURE CAPTIONS

Fig. 1. (a) Optical absorption spectra before (curve 1) and after (curve 2) X-ray irradiation, excitation (Exc) spectra (curves 3 and 4), and emission (Emi) spectra (curves 5, 6 and 7) of the Ag-activated glass after X-ray irradiation. (b) Time-resolved RPL spectra of X-ray-irradiated Ag-activated glass with an excitation of 355 nm.

Fig. 2. Schematic diagram of a compact disk-type RPL glass imaging system.

Fig. 3. Dose dependence of the RPL amplitude from the Ag-activated glass irradiated with X-rays. The RPL image under a black light of X-ray-irradiated glass was shown in the inset.

Fig. 4. RPL line pattern and line-width values taken using the homemade rotating acquisition system at a rotating speed of 400 rpm. A schematic view of the spatial resolution measurement is shown in the inset.

Fig. 5. (a-1), (a-2) Photoimages of the mask used for X-ray irradiation. (b-1), (b-2) RPL images of the X-ray irradiated glass detector illuminated by a black light at 352 nm. (c-1), (c-2) Reconstructed 2-D dose distribution and 3-D image, respectively.

References

Akselrod, M. S., Yoder, R. C., Akselrod, G. M., 2006a. Confocal fluorescent imaging of tracks from heavy charged particles utilising new Al_2O_3:C,Mg crystals. Radiat. Prot. Dosim. 119 (1-4), 357-362.

Akselrod, G. M., Akselrod, M. S., Benton, E. R., Yasuda, N., 2006b. A novel Al_2O_3 fluorescent nuclear track detector for heavy charged particles and neutrons. Nucl. Instr. and Meth. B 247 (2), 295-306.

Baldacchini, G., Bonfigli, F., Faenov, A., Flora, F., Montereali, R. M., Pace, A., Pikuz, T., Reale, L., 2003. Lithium fluoride as a novel X-ray image detector for biological μ-world capture, J. Nanosci. Nanotech. 3 (6), 483-486.

Bonfigli, F., Faenov, A. Ya., Flora, F., Marolo, T., Montereali, R. M., Nichelatti, E., Pikuz, T. A., Reale, L., Baldacchini, G., 2005. Point defects in lithium fluoride films for micro-radiography, X-ray microscopy and photonic applications. Phys. Status Solidi (A) 202 (2), 250-255.

Knežević, Ž., Beck, N., Milković, Đ., Miljanić, S., Ranogajec-Komor, M., 2011. Characterisation of RPL and TL dosimetry systems and comparison in medical dosimetry applications, Radiat. Meas. 46 (2), 1582-1585.

Kurobori, T., Zheng, W., Miyamoto, Y., Nanto, H., Yamamoto, T., 2010. The role of silver in the radiophotoluminescent properties in silver-activated phosphate glass and sodium chloride crystal. Opt. Mater. 32 (9), 1231-1236.

Lee, J. H., Lin, M. S., Hsu, S. M., Chen, I. J., Chen, W. L., Wang, C. F., 2009. Dosimertry characteristics and performance comparisons: Environmental radiophotoluminescent glass dosemeters versus thermoluminescent dosemeters, Radiat. Meas. 44 (1), 86-91.

Maki, D., Nagai, T., Sato, F., Kato, Y., Yamamoto, T., Iida, T., 2011. Microscopic dose measurement with thin radiophotoluminescence glass plate. Radiat. Meas. 46 (2), 1543-1546.

Oberhofer, M., Scharmann, A., 1979. Applied Thermoluminescent Dosimetry. Adam Hilger, Bristol.

Olko, P., 2010. Advantages and disadvantages of luminescence dosimetry. Radiat. Meas. 45 (3-6), 506-511.

Perry, J. A., 1987. RPL Dosimetry, Medical Science Series. Adam Hilger, Bristol and Philadelphia.

Pikuz, T., Faenov, A., Fukuda, Y., Kando, M., Bolton, P., Mitrofanov, A., Vinogradov, A., Nagasono, M., Ohashi, H., Yabashi, M., Tono, K., Senba, Y. , Togashi, T., Ishikawa, T., 2012. Optical features of a LiF crystal soft x-ray imaging detector irradiated by free electron laser pulses. Opt. Express 20 (4), 3424-3433.

Ranogajec-Komor, M. , Knežević, Ž., Miljanić, S., Vekić, B., 2008. Characterisation of radiophotoluminescent dosimeters for environmental monitoring. Radiat. Meas. 43 (2-6), 392-396.

Sato, F., Kuchimaru, T., Ikeda, T., Shimizu, K., Kato, Y., Yamamoto, T., Iida, T., 2008. X-ray microbeam measurement with radiophotoluminescent glass plate for single cell irradiation. Radiat. Meas. 43 (2-6), 912-916.

Sonoda, M., Takano, M., Miyahara, J., Kato, H., 1983. Computed radiography utilizing scanning laser stimulated luminescence, Radiology 148 (3), 833-838

Yukihara, E. G., McKeever, S. W. S., 2011. Optically Stimulated Luminescence, John Wiley & Sons.

Zhao, C., Kurobori, T., Miyamoto, Y., Yamamoto, T., 2011. Properties of a novel radiophotoluminescent readout system using a cw modulated UV laser diode and phase-sensitive technique, Radiat. Meas. 46 (2), 1571-1573.

Zheng, W., Kurobori, T., 2011a. Assignments and optical properties of X-ray-induced colour centres in blue and orange radiophotoluminescent silver-activated glasses. J. Lumin. 131 (1), 36-40.

Zheng, W., Kurobori, T., Miyamoto, Y., Nanto, H., Yamamoto, T., 2011. Formation and assignment of silver defect centres in phosphate glass induced by femtosecond laser pulses. Radiat. Meas. 46 (2), 1402-1405.

Zheng, W., Kurobori, T., 2011b. Observation and partly characterisation of silver nanoparticles in X-ray irradiated radiophotoluminescent phosphate glass, Nucl. Instr. and Meth. B 269 (23), 2814-2818.

Single column
90 mm width

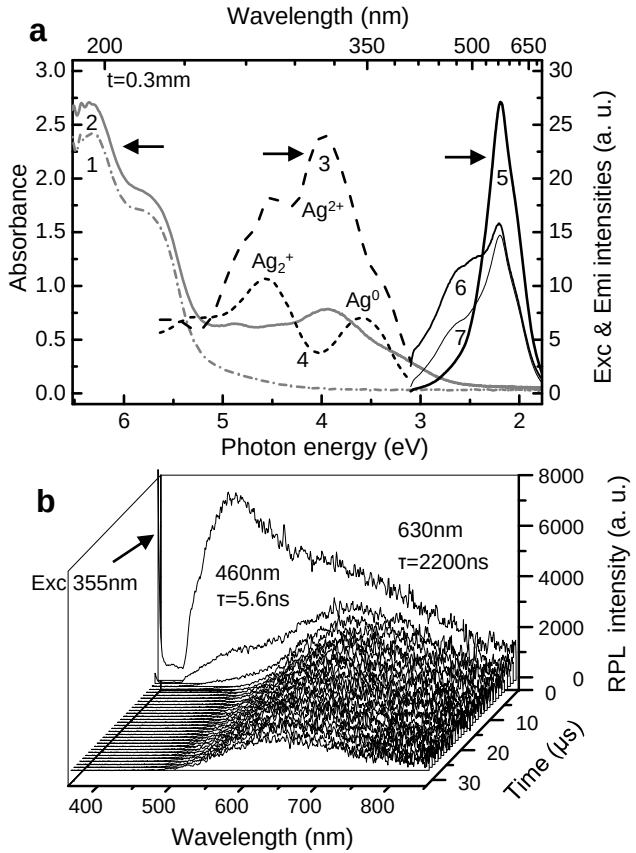

Fig. 1
T.Kurobori

Single column
90 mm width

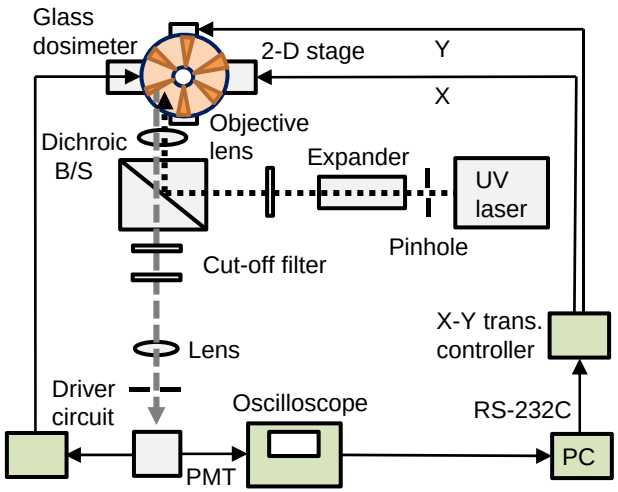

Fig. 2
T.Kurobori

Single column
90 mm width

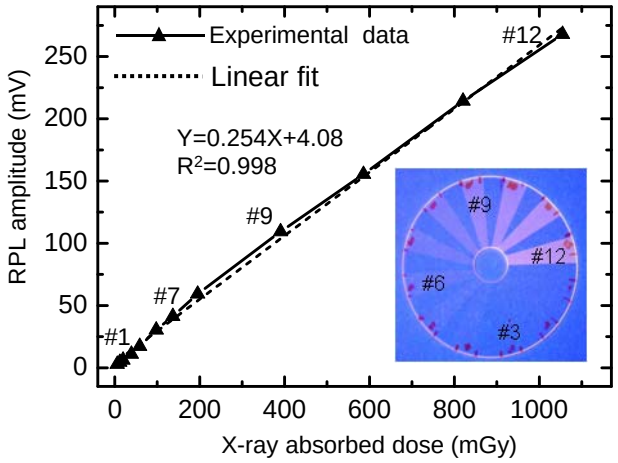

Fig. 3
T.Kurobori

Single column
90 mm width

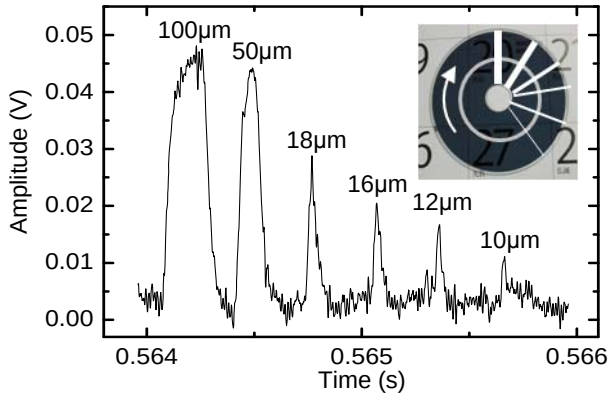

Fig. 4
T.Kurobori

1.5 column
140 mm width

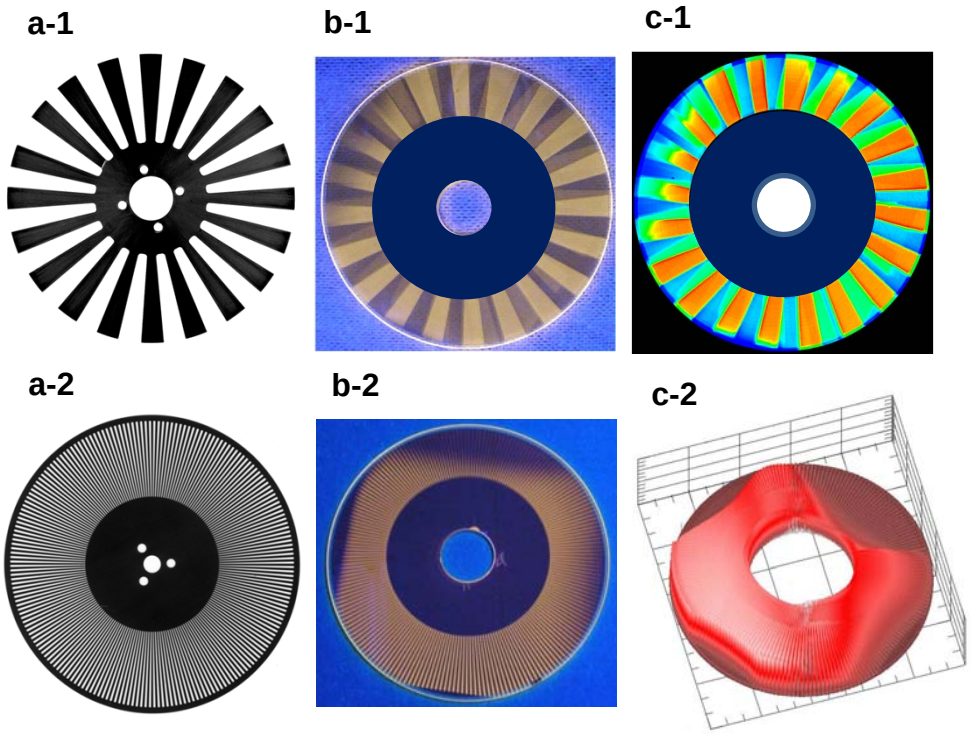

Fig. 5
T.Kurobori